Electronic Supplementary Information (ESI)

A multifunctional coumarin-based probe for distinguishable detection of Cu^{2+} and Zn^{2+}: Its piezochromic, viscochromic and AIE behaviour with real sample analysis and bio-imaging applications

Aayoosh Singh[a], Pranjalee Yadav[a], Saumya Singh[a], Pradeep Kumar[b], S. Srikrishna[b], Vinod P. Singh[a*]

[a]*Department of Chemistry, Institute of Science, Banaras Hindu University, Varanasi-221005, India*

[b]*Department of Biochemistry, Banaras Hindu University, Varanasi-221005, India*

Table of Contents

Experimental

Reagents

All compounds and reagents were obtained from commercial sources and used without additional purification. All the metal salts and solvents were purchased from Merck Chemicals, India. 2, 4-dihydroxybenzaldehyde, ethyl aceto- acetate, thiophene-2-carbohydrazide, and piperidine were bought from Sigma-Aldrich Chemicals, USA. All the studies were conducted with Millipore water. One of the reactants 3-acetyl-7-hydroxy-2H-chromen-2-one was synthesized by the reported procedure.[1]

Synthesis of *(E)*-N'-(1-(7-hydroxy-2-oxo-2H-chromen-3-yl)ethylidene)thiophene-2-carbohydrazide (CTH)

The Schiff base, *(E)*-N'-(1-(7-hydroxy-2-oxo-2H-chromen-3-yl)ethylidene)thiophene-2-carbohydrazide (**CTH**) was synthesized by a condensation reaction between 3-acetyl-7-hydroxy-2H-chromen-2-one (10 mmol, 2.04 g) and thiophene-2-carbohydrazide (10 mM, 1.42 g) in 25 mL ethanol. A pale white compound was obtained after refluxing the reactants for 2 h in a round bottom flask. The product was filtered, washed several times with ethanol and dried in a desiccator

over anhydrous calcium chloride. The progress of the reaction was monitored by thin-layer chromatography (TLC) using ethyl acetate and hexane (1:4, v/v) (Scheme 1).

Analytical data: pale white powder, yield 87%. M.P. 254 °C, HRMS calculated for $C_{16}H_{12}N_2O_4S$: m/z [M^+] 328.0518 found m/z [M + H]$^+$ 329.0575; [M + Na]$^+$ 351.0392. IR (KBr, cm^{-1}): ν(OH) 3471, ν(NH) 3241, 3169, $\nu(C{=}O)_{lactone\ ring}$ 1692, $\nu(C{=}O)_{amide}$ 1659, ν(C=N) 1629. ^{1}H NMR (500 MHz, DMSO-D_6): δ 11.00 (1H, -OH), 10.72 (1H, -NH), 8.14 (1H, Ar-H), 8.00 (1H, Ar-H), 7.83 (1H, Ar-H), 7.65 (1H, Ar-H), 7.14 (1H, Ar-H), 6.79 (1H, Ar-H), 6.73 (1H, Ar-H), 2.24 (3H,–CH_3). ^{13}C NMR (126 MHz, DMSO-D_6): δ 162.46 (>$C{=}O_{amide}$), 160.23 (>$C{=}O_{lactone\ ring}$), 156.13 (>C-OH), 150.15 (>C=N), 142.68, 132.66, 131.21, 129.67, 122.68, 116.80, 115.40, 115.07, 114.22, 111.81, 102.36 (aromatic carbons), 16.75 (-CH_3).

Synthesis of CTH-Cu^{2+} complex

The **CTH**-Cu^{2+} complex was synthesized by adding 50 mL of ethanolic solution of **CTH** (1 mmol, 0.328 g) into 50 mL of ethanolic solution of $Cu(NO_3)_2.3H_2O$ (1 mmol, 0.241 g) drop wise in a round bottom flask in 1:1 (M:L) molar ratio. After 4 h of stirring the reaction mixture at room temperature, a dark green precipitate was formed. The precipitate was filtered and washed several times with ethanol and finally with diethyl ether. The complex thus obtained was vacuum dried over anhydrous $CaCl_2$. The dark green single crystals of the complex suitable for X-ray crystallography were obtained when 1 equiv. of NH_4PF_6 was added in a saturated solution of **CTH**-Cu^{2+} in DMSO-MeOH (1:1, v/v) to stabilise the cationic complex and the resulting solution was slowly evaporated.

Analytical data: dark green, yield: 57%. M.P. >300 °C. HRMS calculated for $C_{18}H_{19}CuN_2O_6S_2$: m/z [M^+] 485.9981 found m/z [M]$^+$ 486.2328. IR (KBr, cm^{-1}): ν(OH) 3443, $\nu(C{=}O)_{lactone\ ring}$ 1650, $\nu(>C{=}N)_1$ 1604, $\nu(>C{=}N)_2$ 1566, $\nu(C\text{-}O^-)$ 1384.

Synthesis of CTH-Zn^{2+} complex

The **CTH** ligand (1 mmol, 0.328 g) was first dissolved in minimal quantity of DMSO and then diluted with 50 mL ethanol. This solution was gradually added to 50 mL ethanolic solution of $Zn(NO_3)_2.3H_2O$ (1 mmol, 0.241 g) in 1:1 (M:L) molar ratio. A dark orange precipitate was formed after stirring the solution for 30 min at room temperature. It was filtered, washed many times with ethanol and finally with diethyl ether, and then dried over anhydrous $CaCl_2$.

Analytical data: dark orange, yield: 83%. M.P. >300 °C. HRMS calculated for $C_{18}H_{17}N_2O_5S_2Zn$: m/z [M^+] 468.9870 found m/z [M]$^+$ 468.9874. IR (KBr, cm^{-1}): ν(OH) 3436, $\nu(C{=}O)_{\text{lactone ring}}$ 1661, $\nu(>C{=}N)_1$ 1601, $\nu(>C{=}N)_2$ 1529, $\nu(C\text{-}O^-)$ 1383.

Physical measurements

KBr pellets were used to record FT-IR spectra in 4000-400 cm^{-1} region on a FT-IR 4700 JASCO spectrophotometer. The JEOL Resonance Inc. multinuclear FT NMR spectrometer (Model-ECZ-500R) was used to obtain ^1H and ^{13}C NMR spectra in DMSO-d_6. The chemical shifts are given in parts per million (ppm) with respect to an internal standard of tetramethylsilane (TMS). At room temperature, ESI-mass spectra were recorded on an HRMS SCIEX X-500R QTOF spectrometer. The Shimadzu UV-1800 spectrophotometer was used to take all the UV-Vis. spectra. Fluorescence spectra were obtained using a Fluromax 4CP plus fluorescence spectrophotometer (slit = 1 nm). The LMPH-10 pH meter was used to monitor and adjust the pH of various solutions. Melting points were measured using a digital melting point apparatus at a heating rate of 10 °C/min. The EVO – (Scanning Electron Microscope) MA15 / 18 were used to capture the SEM images. DLS measurements were conducted on a Zetasizer Ultra (ZSU5700) Malvern Panalytical (UK) Particle Size Analyzer. A Bruker D_8 Advance powder X-ray diffractometer equipped with Cu Kα radiation with a LyneEye detector was used for the powder X-ray diffraction experiments. XtaLAB

Synergy-I was used to acquire single-crystal X-ray diffraction data. Solid state fluorescence was recorded on Fluorolog FL-3C-21 UV-Vis-NIR-Spectrofluorometer with an integrated sphere (Steady-state) Thermal property was analysed by differential scanning calorimetry (DSC) on a Mettler Toledo Model-822e instrument in nitrogen environment at the heating rate of 10 ^{o}C/min.

General procedures

The stock solutions of metal salts and **CTH** (1×10^{-2} M) were prepared in millipore water and DMF, respectively. For various investigations, 20 μM solution of **CTH** was prepared in DMF:H_2O (3:7, v/v, pH 7.4) HEPES buffer solution by further diluting the stock solution. With increasing concentrations of the metal ion solutions (1×10^{-3} M), the **CTH** solution of 1×10^{-2} M concentration was used for the absorption and emission titration experiments. Every titration study was performed at room temperature. Nitrate salts were employed for all of the cations, whereas, acetate and chloride salts of Zn^{2+} and Cu^{2+} were used to test the counter anion changes. For every fluorescence study, the excitation wavelength of 350 nm was optimized.

Fluorescence quantum yield measurements

Quantum yield was calculated by using the following equation:[2]

$$Q = Q_r\left(\frac{I}{I_r}\right)\left(\frac{OD}{OD_r}\right)\left(\frac{n^2}{n_r^2}\right) \quad \ldots \textbf{(1)}$$

Where, Q = fluorescence quantum yield, I = integrated fluorescence intensity, n = refractive index of liquid and OD = optical density (absorption). To indicate the known quantum yield of reference quinine sulphate, the subscript r is used as 0.54 in 0.1 M H_2SO_4.

Fluorescence decay measurements

Time-resolved fluorescence spectra were recorded to explore AIE and sensing properties at the concentrations of 30 μM and 20 μM, respectively.

Dynamic parameters are determined from the following equation:

$$y = A_1 * \exp\left(-\frac{x}{\tau_1}\right) + A_2 * exp\left(-\frac{x}{\tau_2}\right) + y_0 \quad \text{… (2)}$$

Weighted mean lifetime <τ> was calculated by using the following equation:

$$<\tau> = (A_1\tau_1 + A_2\tau_2)/(A_1 + A_2) \quad \text{… (3)}$$

Where, A_1/A_2 and τ_1/τ_2 are the fractions or amplitudes (A) and lifetimes (τ), respectively.

The radiative rate constant (K_r) and non-radiative rate constant (K_{nr}) are calculated from the following equations:[3]

$$<\tau^{-1}> = (K_r + K_{nr}) \quad \text{… (4)}$$

$$K_r = \frac{\phi}{<\tau>} \quad \text{… (5)}$$

Calculation method for limit of detection (LOD)

Using fluorescence titration data, the limit of detection for **CTH** was calculated by the IUPAC definition, which was based on a plot of emission intensity vs increasing Zn^{2+}/Cu^{2+} concentration. To calculate the S/N ratio, we repeated our observations eight times, each time measuring the emission intensity of **CTH** without Zn^{2+}/Cu^{2+} and calculating the standard deviation of blank data. The slope was calculated by plotting fluorescence intensity data at 509 nm against Zn^{2+}/Cu^{2+} concentration. The following equation is used to establish the detection limit:[4]

$$\text{Limit of Detection (LOD)} = \frac{3SD}{Slope(m)} \quad \text{… (6)}$$

In this equation, m represents the slope of intensity vs sample concentration, and SD is the standard deviation of blank measurements.

Calculation method for association constant

The binding ratio of **CTH** to metal ions was calculated using Job's plot and the binding constants (K_a) of **CTH** for Zn^{2+} and Cu^{2+} were obtained using the Benesi-Hildebrand equation.[5]

$$\frac{I_0}{I - I_0} = \frac{a}{b - a}\left(\frac{1}{K_a[Metal]} + 1\right) \quad \ldots$$

(7)

In this equation, I and I_0 are the intensities of **CTH** fluorescence at 509 nm in the presence and absence of Zn^{2+}/Cu^{2+}, respectively; a and b are constants; and [Metal] is the concentration of Zn^{2+}/Cu^{2+}.

Computational details

Using the Gaussian-09 software, 6-311G (d, p) basis set and RB3LYP technique, we performed theoretical computations for the **CTH**, **CTH-**Cu^{2+} and **CTH-**Zn^{2+} complexes. The potential energy surface minima of DFT-optimized structures were validated.[6,7]

X-ray crystallography

Rigaku XtaLAB Synergy-I diffractometer with CrysAlis^{Pro} and a graphite monochromated Mo-Kα (λ= 0.71073) radiation source was used to get the single crystal X-ray diffraction data at 293 K. The structure was solved using SHELXL-97 and improved using complete matrix least-square on F^2 and anisotropic displacement parameters for all non-hydrogen atoms.[8,9] A riding model was used to refine all hydrogen atoms into their geometrically optimal positions. The structure was generated using the MERCURY software and the ORTEP-3 tool for Windows.[10]

Toxicity assay of CTH

A toxicity assay was conducted on wild-type *Drosophila* flies (Oregon R^+ strain). Virgin flies were placed in triplicate vials containing corn meal agar media that had been treated with different concentrations of **CTH**. The concentrations tested were 0.7 μM, 7 μM, 35 μM, 70 μM and 140 μM. The toxicity assay spanned several days. On the 5th day, the parental flies were removed from

the vials to focus specifically on the F1 progeny. The development of F1 offspring was then monitored until they reached 15 days of age. This allowed for the observation and evaluation of any potential toxic effects that **CTH** might have on the F1 of treated flies.

Cell viability assay

In the MTT assay, the viability of cells was evaluated using MTT (3-(4,5-dimethylthiazol-2-yl)-2,5-diphenyltetrazolium bromide) reagent. The experiment involved dissecting the third instar larval gut of both **CTH**-treated and untreated Oregon R^+ flies under ice-cooled conditions in 1X PBS. Each group consisted of 10 guts, with the untreated group reflecting as the control. The dissected tissues were then individually incubated with 0.6 mg/mL MTT in MCT tubes for 1 h. Metabolically active cells convert MTT into formazan crystals, reflecting their viability. After incubation, the tissues were washed with 1X PBS to remove any unreacted MTT. The tissues were treated with DMSO (dimethyl sulfoxide) to dissolve the crystals and quantify the formazan crystals formed. The mixture was then centrifuged at 10,000 rpm for 10 min at room temperature to separate the dissolved formazan from the tissue debris. A multimode plate reader was used at a wavelength of 750 nm to measure the optical density (OD) of the formazan solution.

Fluorescence response of CTH probe in *Drosophila* larval gut tissue

The procedure involved the dissection of the larval gut tissue in ice-cooled 1X PBS, followed by fixation with 4% PFA for 20 minutes. Subsequently, the tissue was washed with 1X PBS three times, for 15 min. Next, the tissue was divided into four distinct groups and subjected to separate incubation conditions: **CTH** alone, **CTH**-Zn^{2+}, **CTH**-Cu^{2+}, and **CTH** in the presence of both Zn^{2+} and Cu^{2+}. The incubation was performed for 30 min at room temperature. After completion of the incubation period, the tissue was further washed with 1X PBS three times, each wash for five

minutes. After that tissue was mounted on glass in a Mowiol mounting medium and images were captured by the fluorescent microscope (Nikon Eclipse Ni).

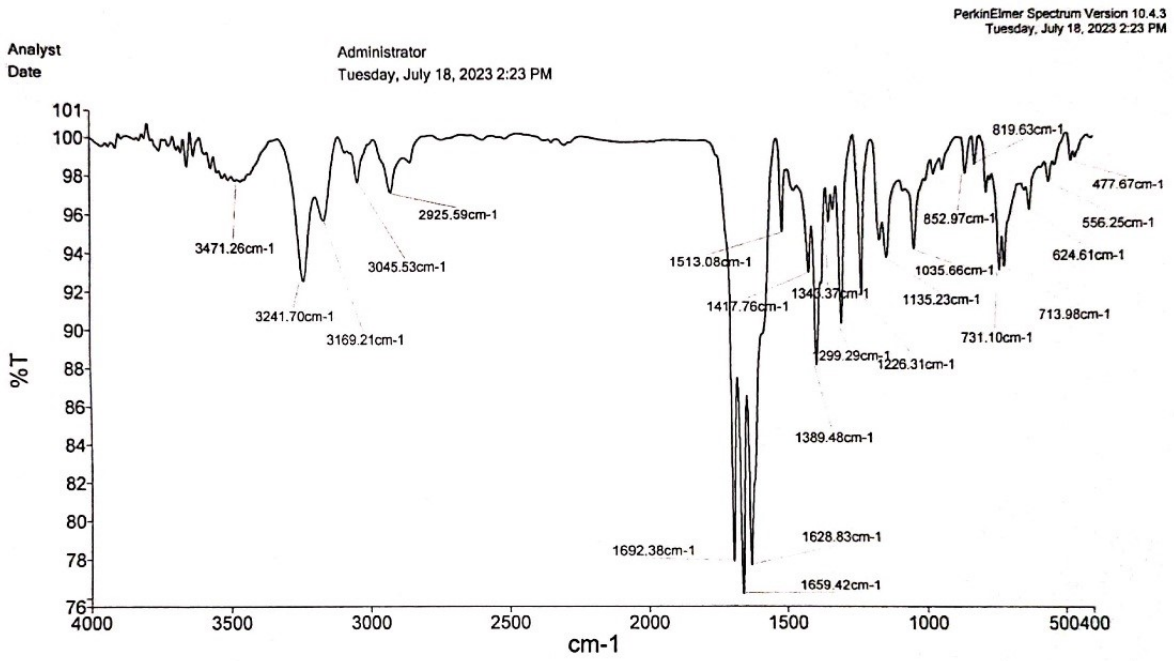

Fig. S1 IR spectrum of **CTH**

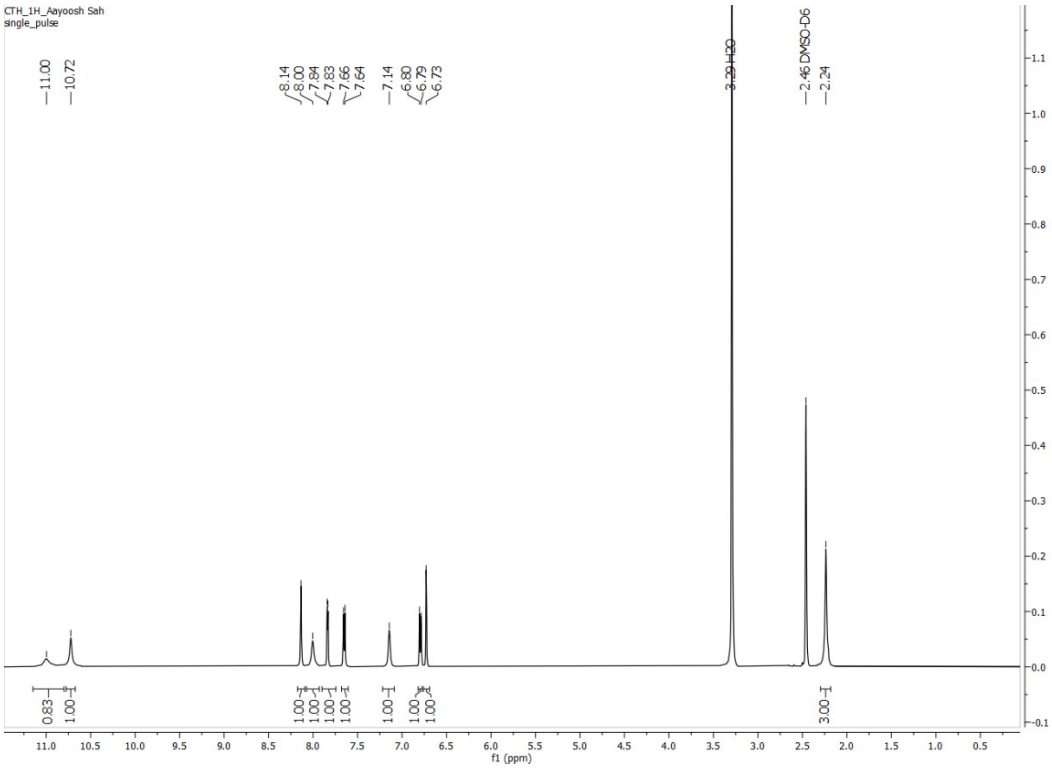

Fig. S2 ^{1}H NMR spectrum of **CTH**

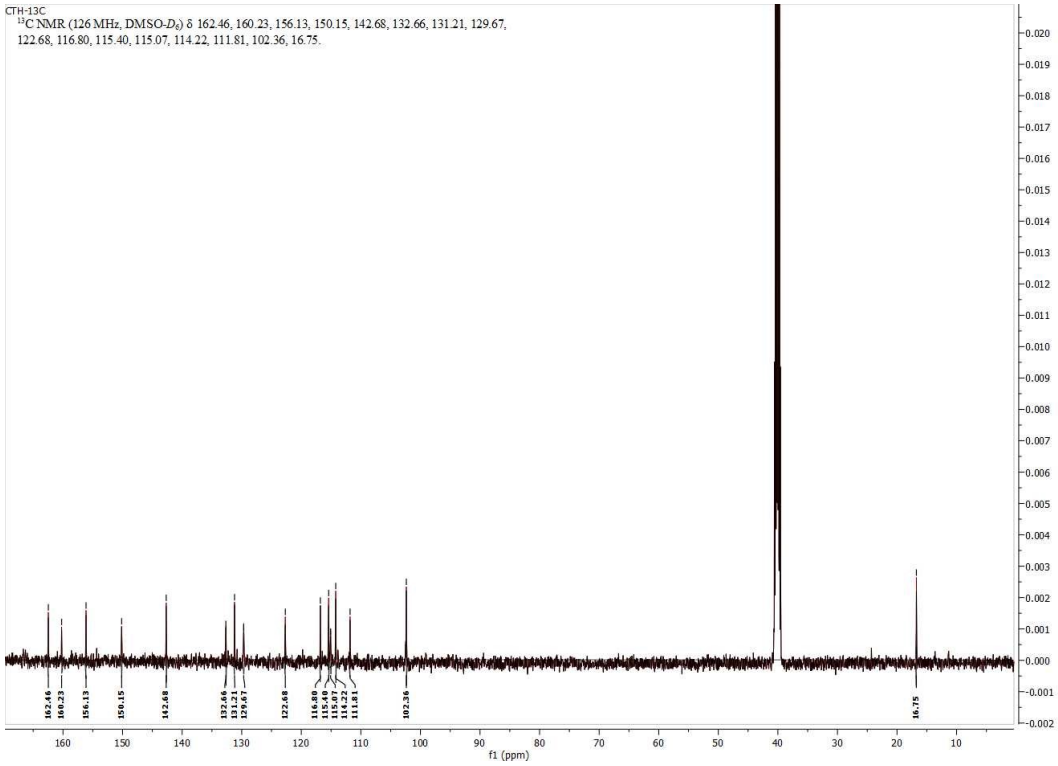

Fig. S3 ^{13}C NMR spectrum of **CTH**

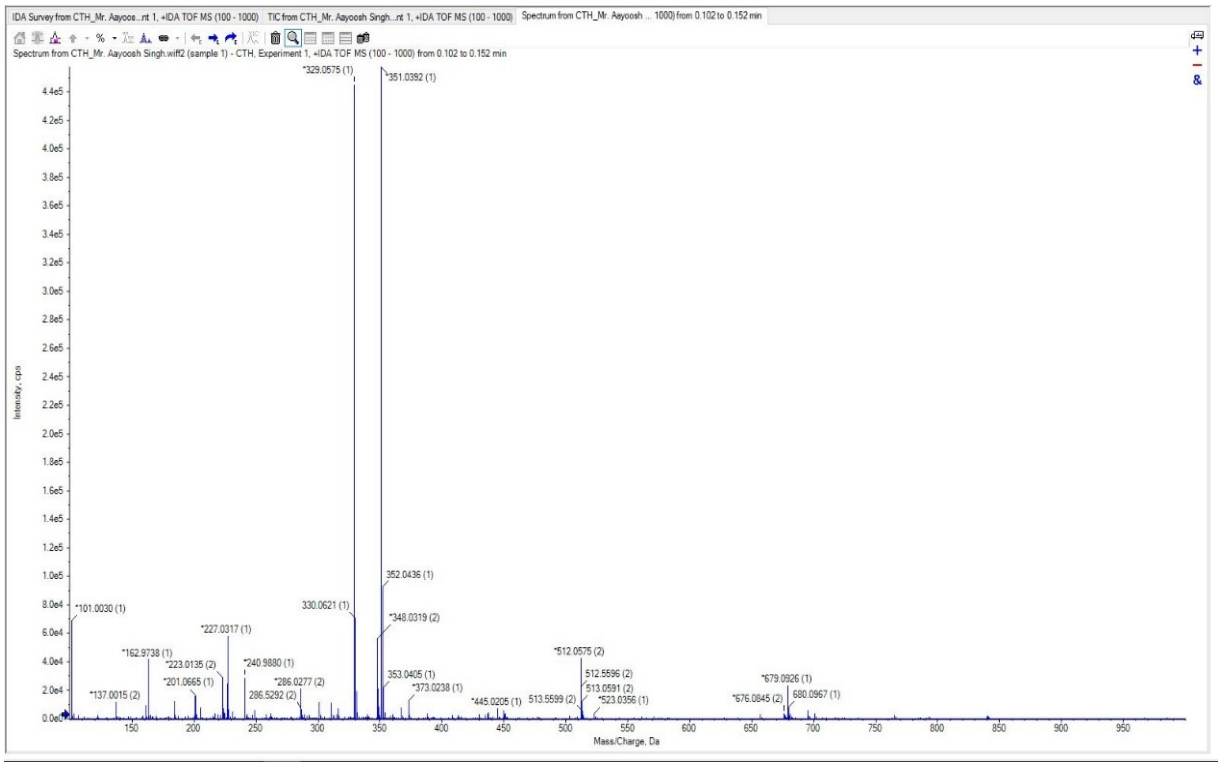

Fig. S4 Mass spectrum of **CTH**

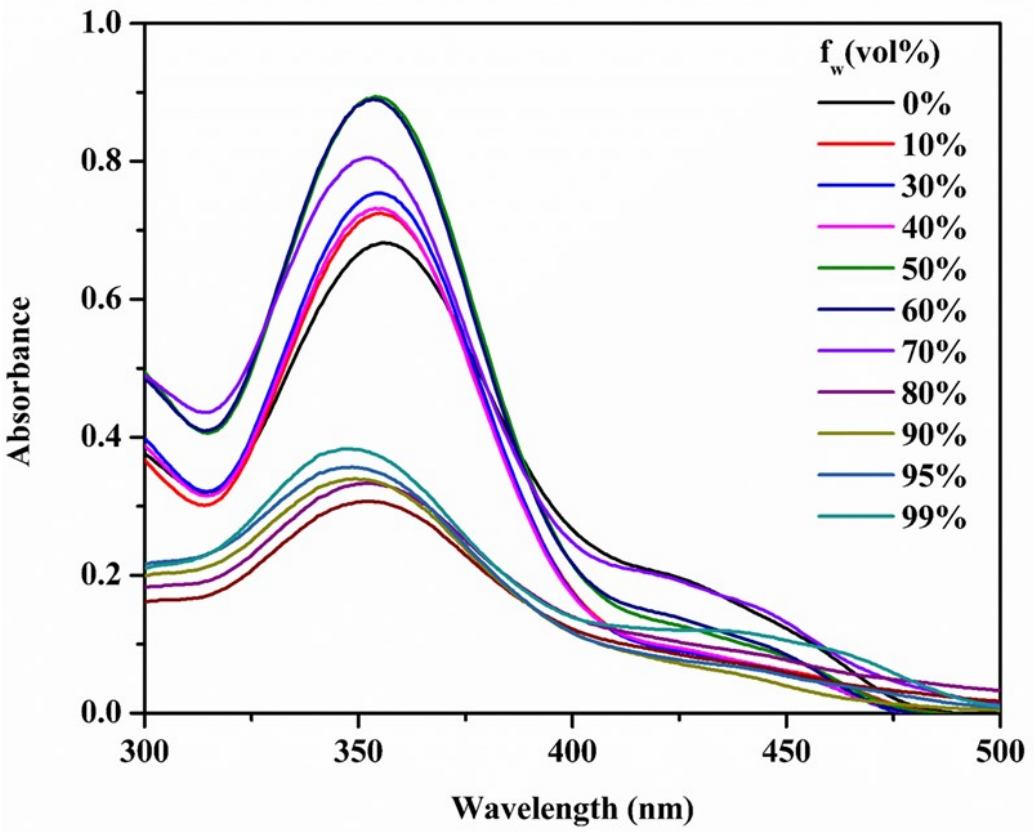

Fig. S5 Absorbance spectra of 30 μM **CTH** at varying ethanol–water fraction.

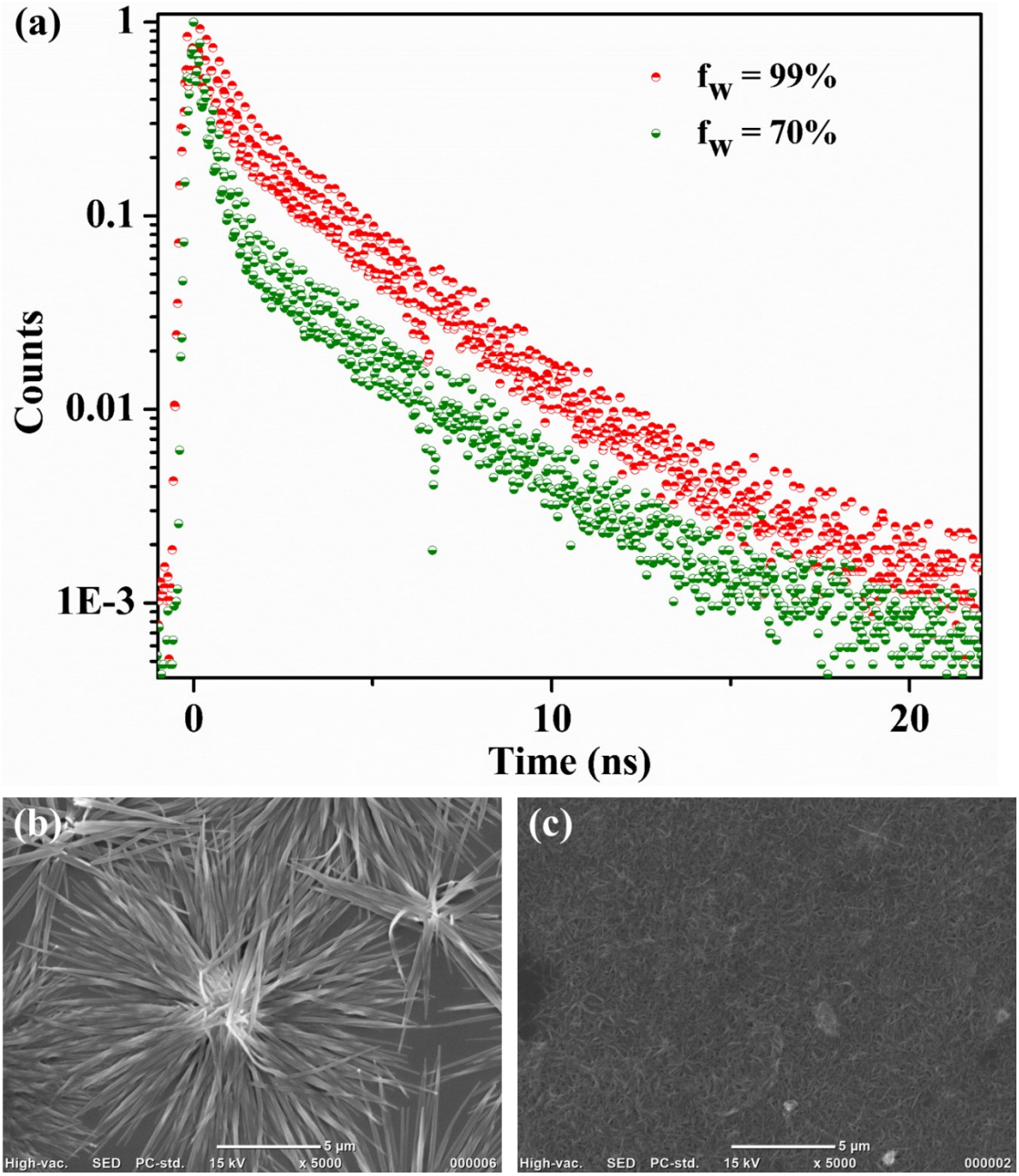

Fig. S6 (a) CTH fluorescence lifetime spectra at varying water contents; **(b)** Aggregates of **CTH** (30 µM) as seen by scanning electron microscopy in ethanol-water solutions f_w = 70%; **(c)** f_w = 95%.

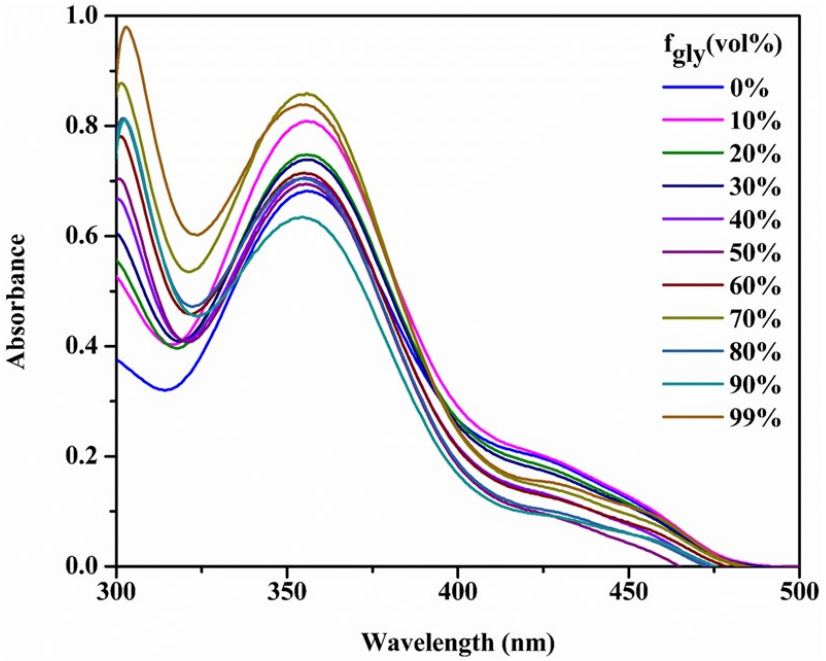

Fig. S7 Absorbance spectra of 30 μM **CTH** at varying ethanol–glycerol fraction.

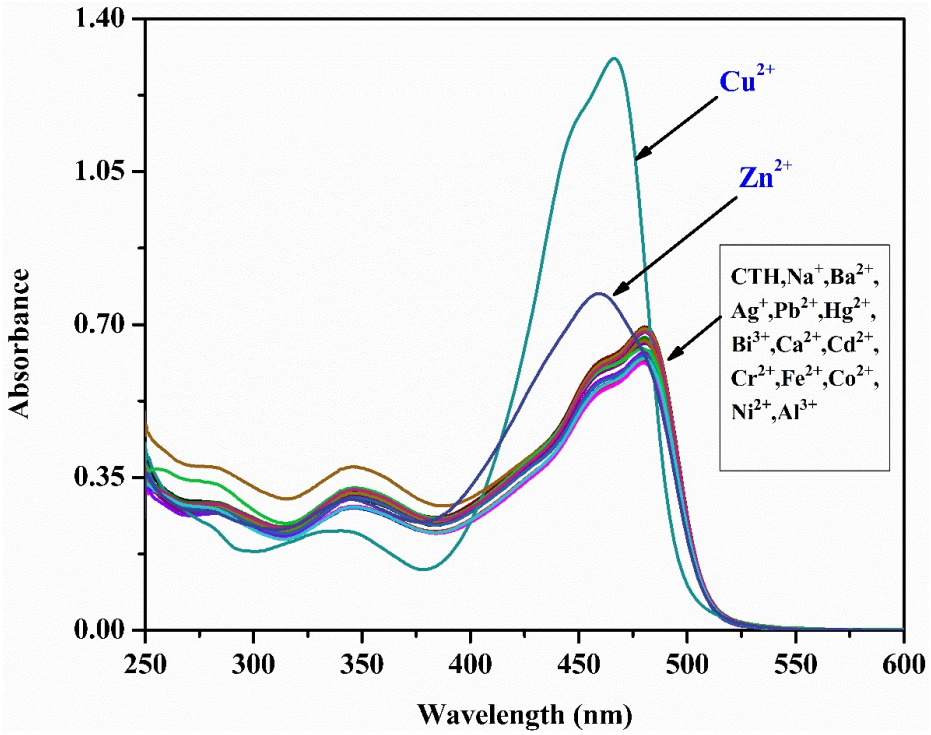

Fig. S8 Absorbance spectra of **CTH** (20 μM) in the presence of other cations (2 equiv.) in DMF:H_2O (3:7, v/v, pH 7.4) HEPES buffer solution.

Fig. S9 Visible colour responses of **CTH** in the presence of various metal ions.

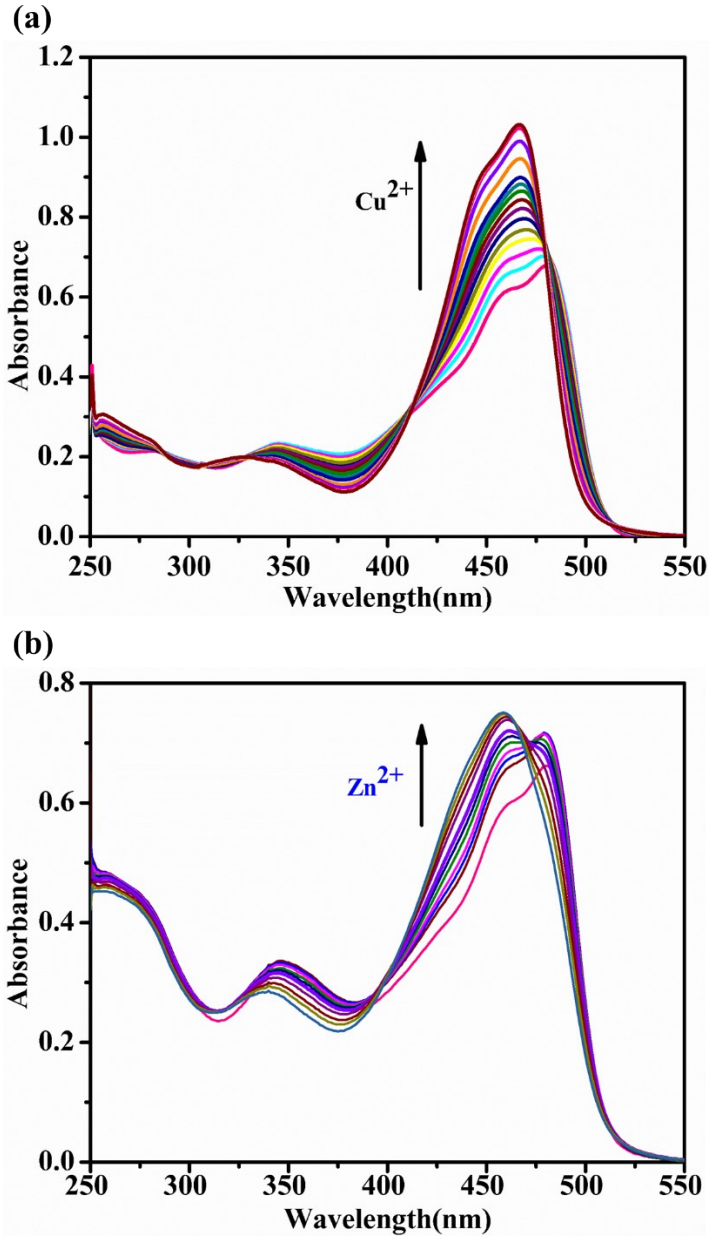

Fig. S10 Absorbance titration spectra of **CTH** (20 μM) in DMF:H_2O (3:7, v/v, pH 7.4) HEPES buffer solution **(a)** in the presence of increasing Cu^{2+} (0-1equiv.) concentration; **(b)** in the presence of increasing Zn^{2+} (0-1equiv.) concentration.

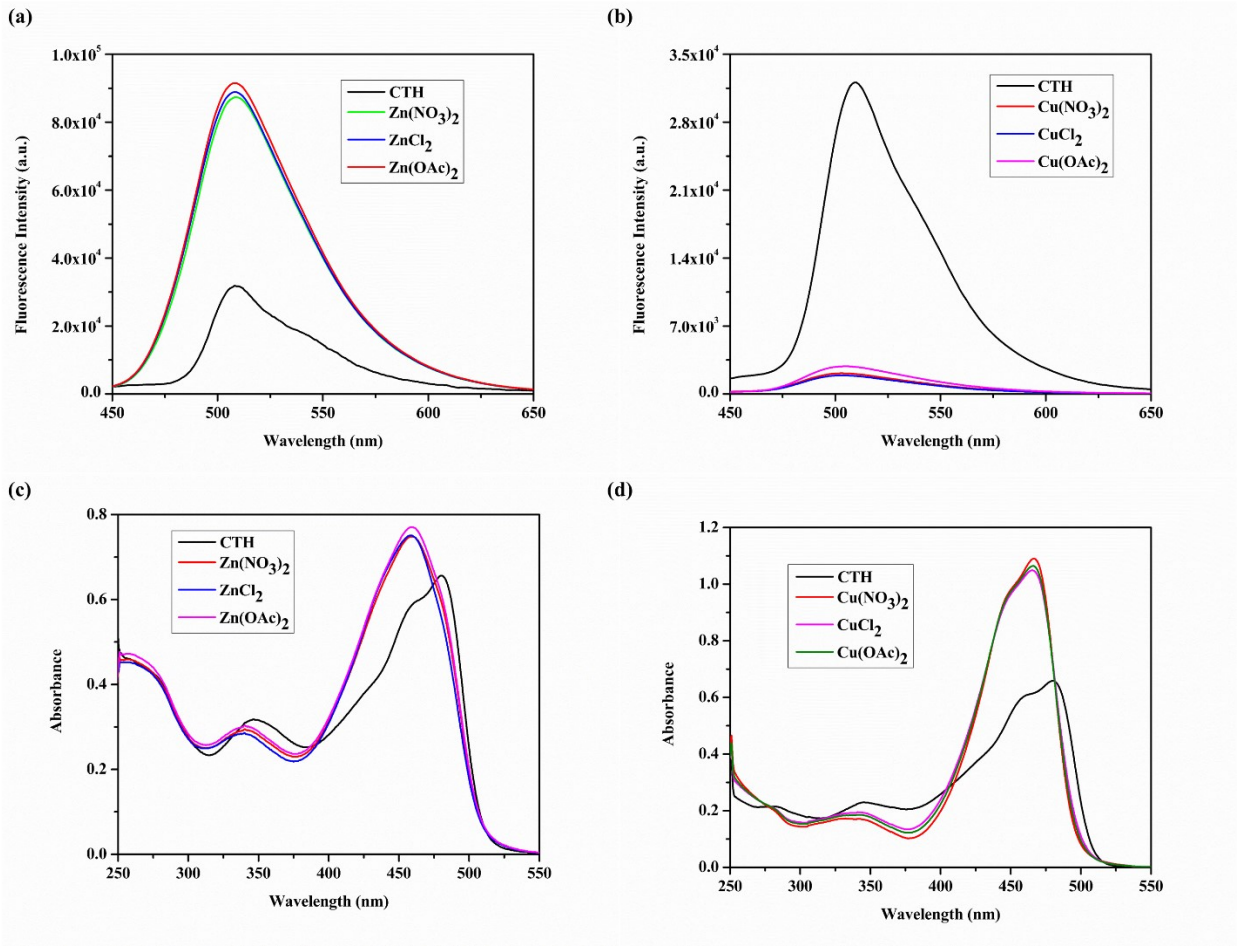

Fig. S11 (a) Fluorescence spectra of **CTH** after addition of Zn^{2+} with different counter anions in DMF:H_2O (3:7, v/v, pH 7.4) HEPES buffer solution. **(b)** Fluorescence spectra of **CTH** after addition of Cu^{2+} with different counter anions in DMF:H_2O (3:7, v/v, pH 7.4) HEPES buffer solution. **(c)** Absorbance spectra of **CTH** after addition of Zn^{2+} with different counter anions in DMF:H_2O (3:7, v/v, pH 7.4) HEPES buffer solution. **(d)** Absorbance spectra of **CTH** after addition of Cu^{2+} with different counter anions in DMF:H_2O (3:7, v/v, pH 7.4) HEPES buffer solution.

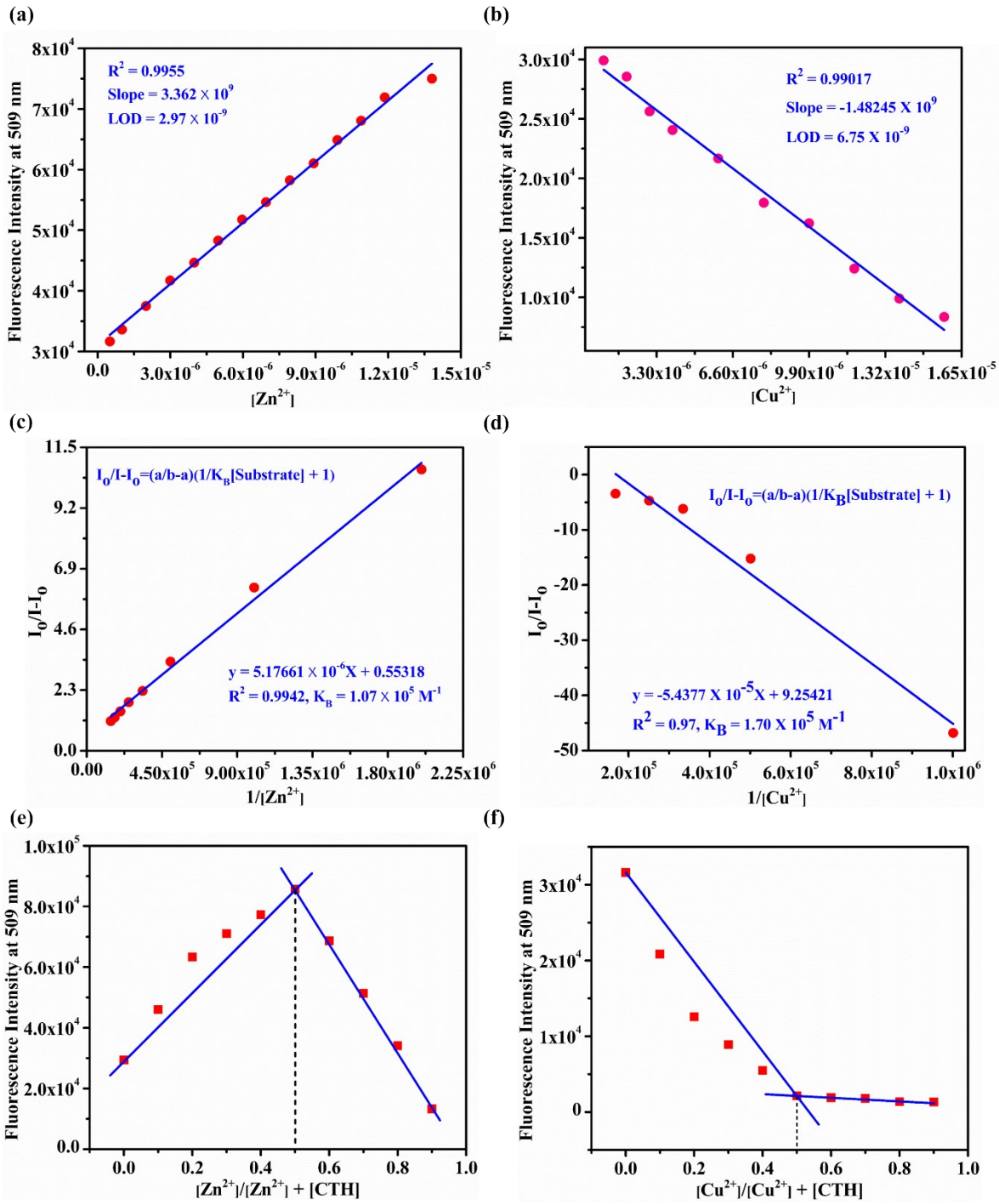

Fig. S12 (a) Limit of detection (LOD = 3σ/Slope) curve plot, the change in fluorescence intensity at 509 nm of **CTH** (20 μM) as a function of Zn^{2+} ions concentration and **(b)** as a function of Cu^{2+} ions concentration. **(c)** Benesi-Hildebrand plot of **CTH** for determination of binding constant with Zn^{2+} and **(d)** for binding constant with Cu^{2+}. R^2 denotes Goodness of fit. (λ_{em} = 509 nm, λ_{ex} = 350 nm). **(e)** Job's plot for determination of binding stoichiometry for **CTH**-Zn^{2+} and **(f)** binding stoichiometry of **CTH**-Cu^{2+}.

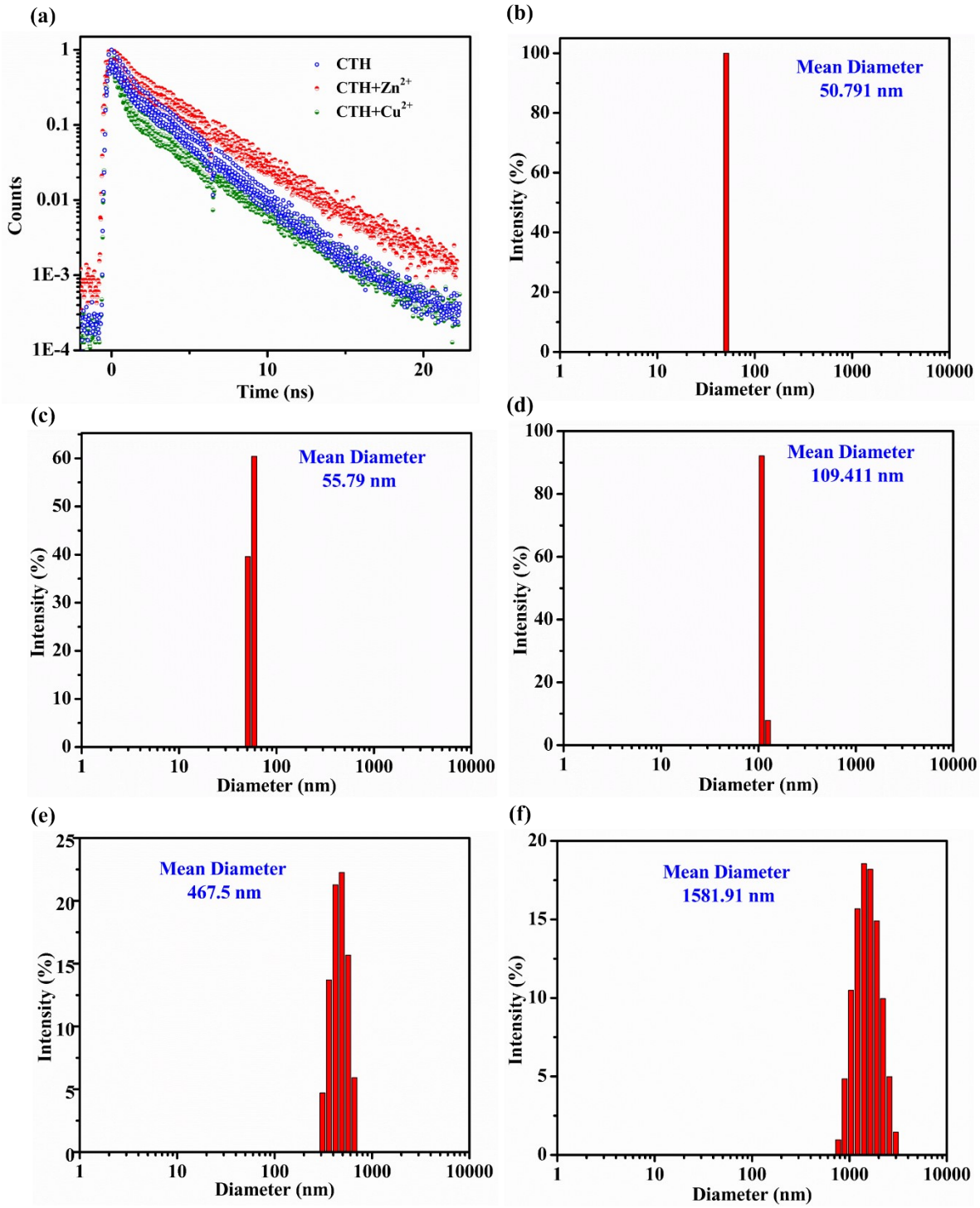

Fig. S13 (a) Time-resolved fluorescence decay profile of **CTH** in absence and presence of Zn^{2+}/Cu^{2+}, respectively in DMF:H_2O (3:7, v/v, pH 7.4) HEPES buffer solution; DLS-based particle size analysis upon addition of Zn^{2+}/Cu^{2+} to **CTH** in DMF:H_2O (3:7, v/v, pH 7.4) HEPES buffer solution **(b) CTH** only; **(c)** addition of 1 equiv. of Zn^{2+} to **CTH (d)** addition of 1 equiv. of Cu^{2+} to **CTH**; **(e)** addition of excess of Zn^{2+} to **CTH (f)** addition of excess of Cu^{2+} to **CTH**.

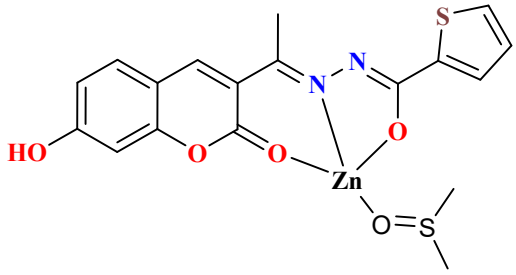

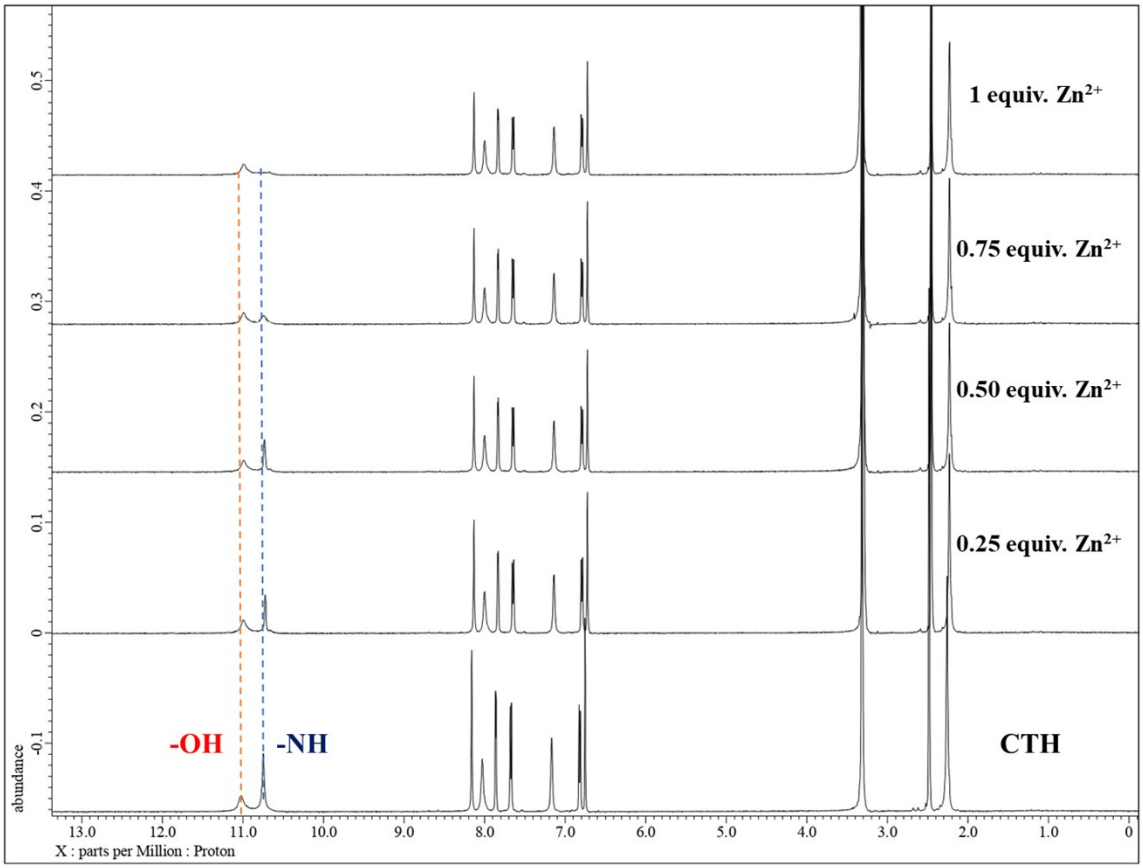

Fig. S14 ^{1}H NMR titration of **CTH** after addition of Zn^{2+} (0-1 equiv.) in DMSO–d_6.

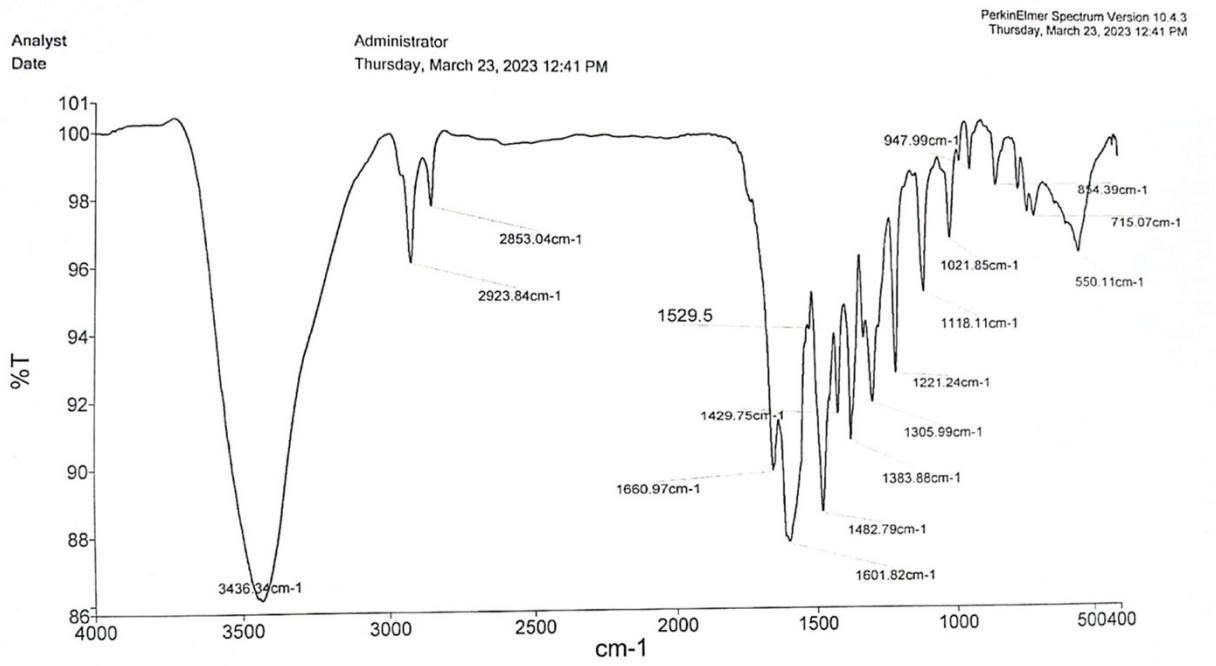

Fig. S15 IR spectrum of **CTH**-Zn^{2+} complex.

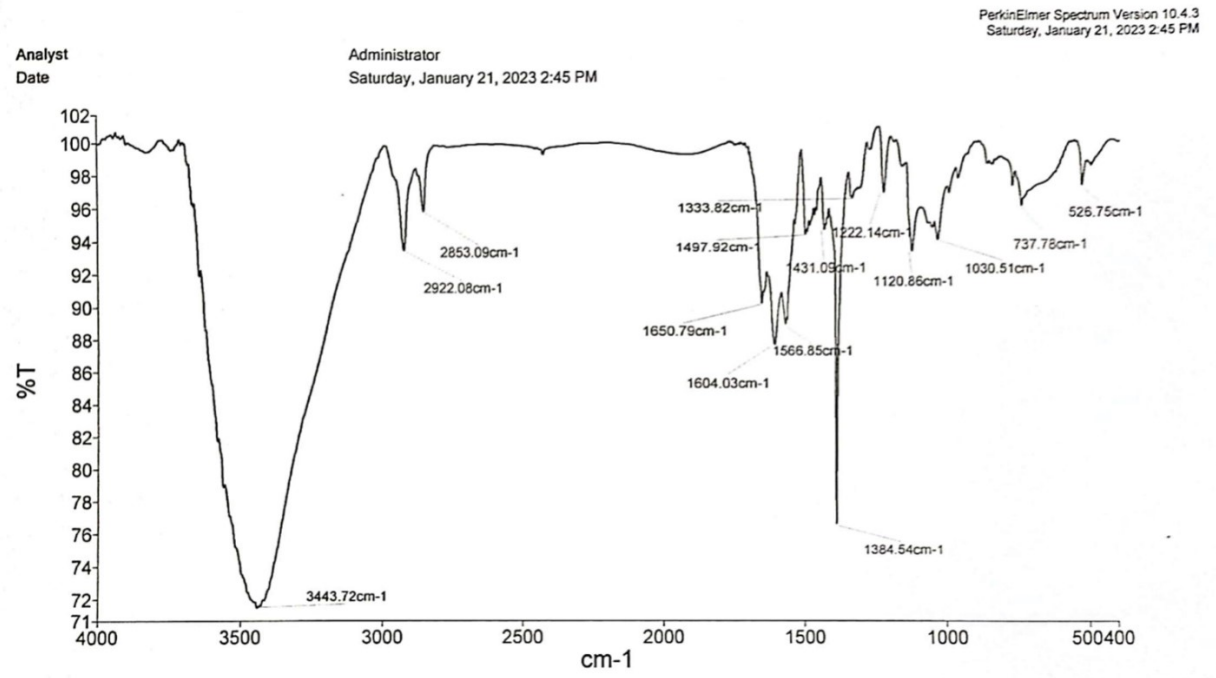

Fig. S16 IR spectrum of **CTH**-Cu^{2+} complex.

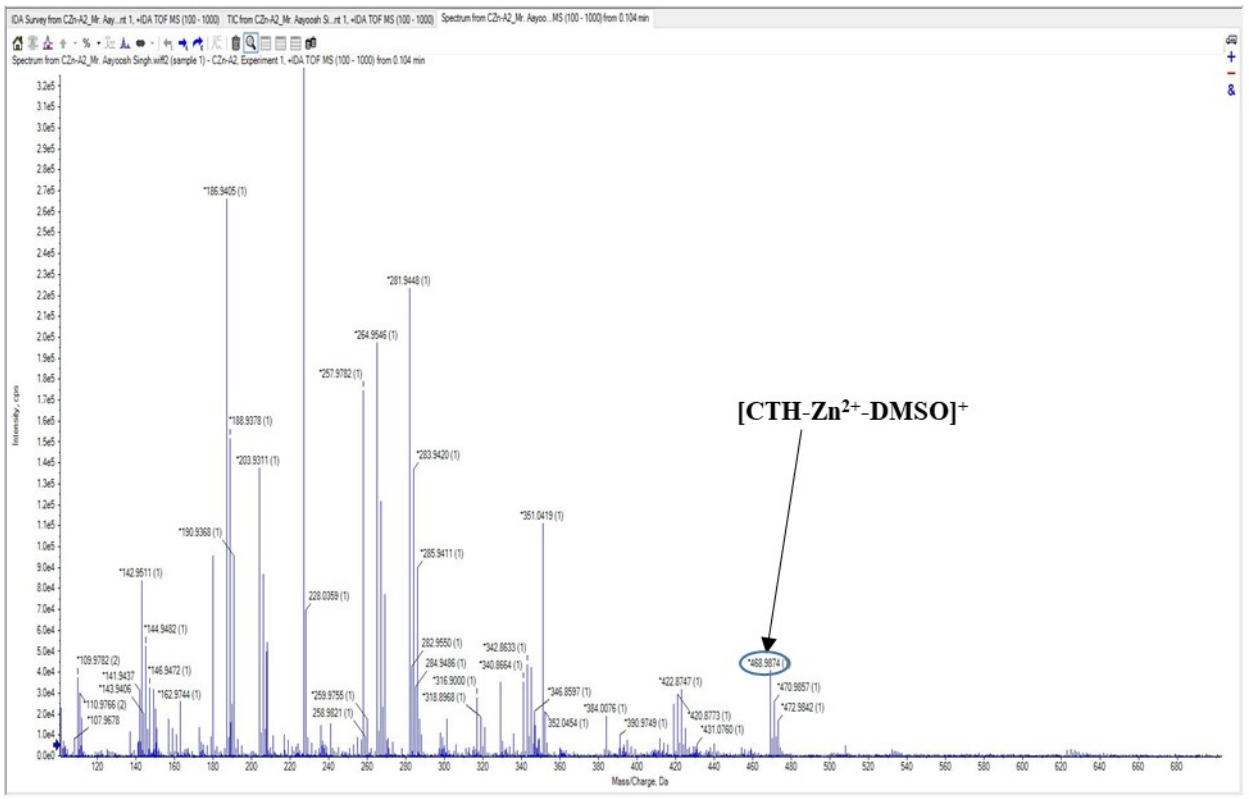

Fig. S17 Mass spectrum of **CTH**-Zn^{2+} complex.

(a)

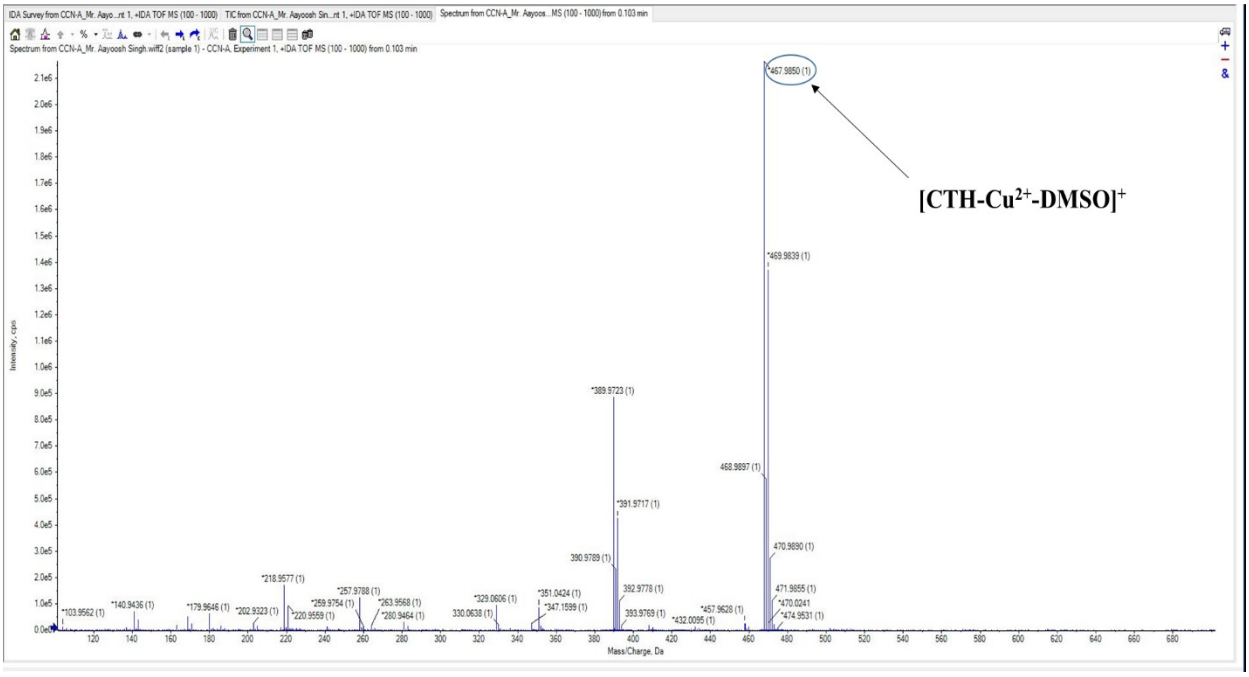

(b)

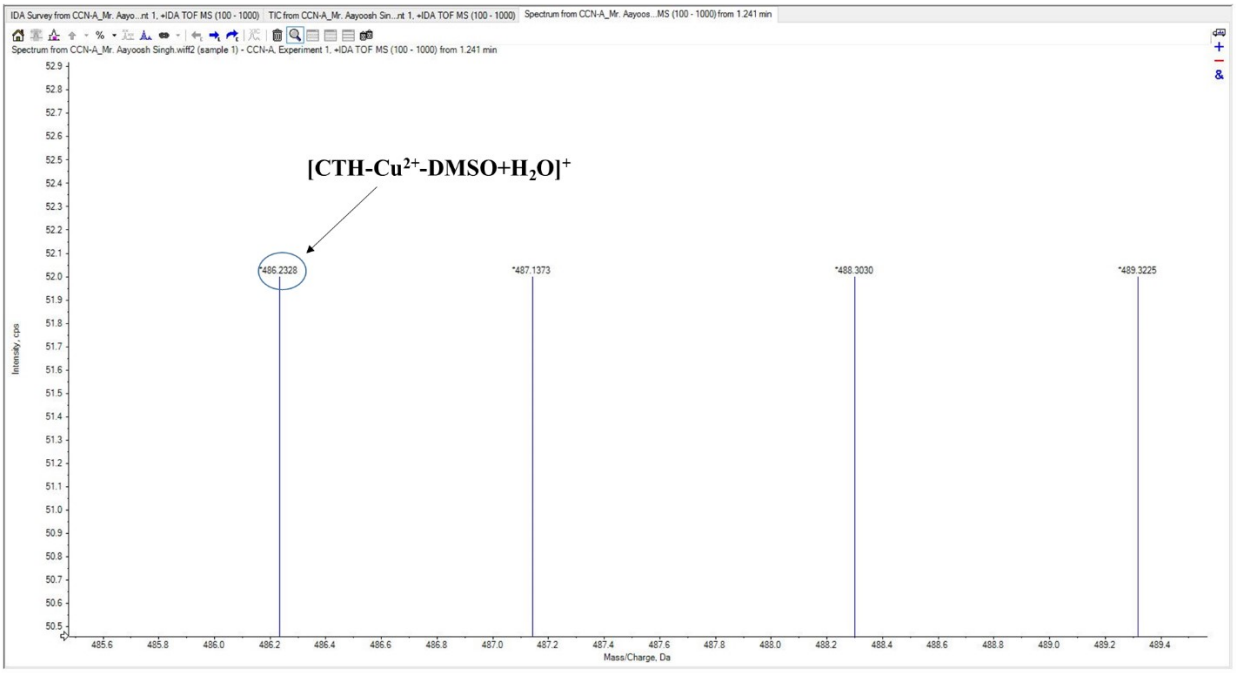

Fig. S18 (a) Mass spectrum of **CTH**-Cu^{2+} complex, **(b)** Molecular ion peak at m/z=486.

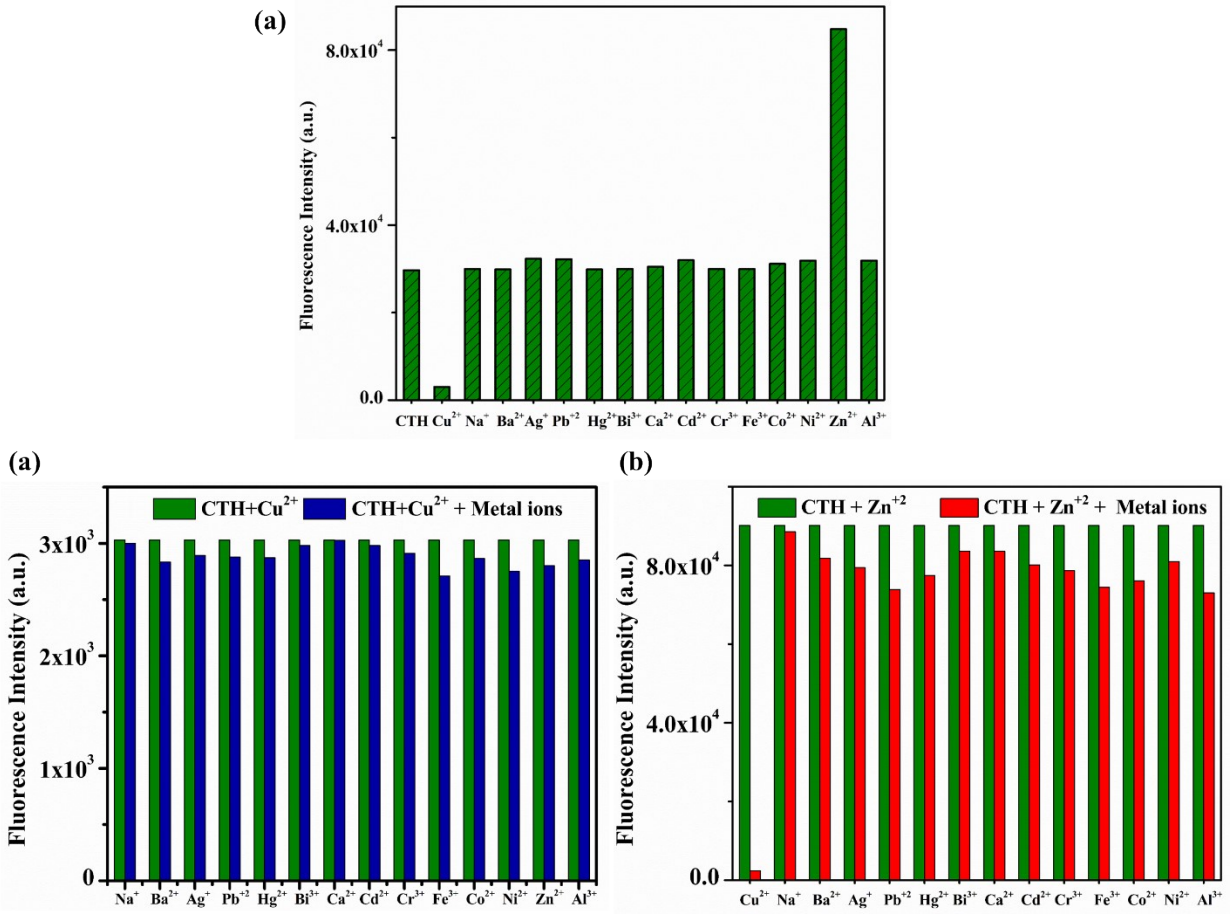

Fig. S19 Fluorescence intensity measurement of **CTH** (20 μM) **(a)** after addition of various metal ions (20 μM) in DMF:H_2O (3:7, v/v, pH 7.4) HEPES buffer solution **(b)** in the presence of Cu^{2+} (20 μM) with addition of other metal ions (20 μM) in DMF:H_2O (3:7, v/v, pH 7.4) HEPES buffer solution **(c)** in the presence of Zn^{2+} (20 μM) with addition of other metal ions (20 μM) in DMF:H_2O (3:7, v/v, pH 7.4) HEPES buffer solution. (λ_{em} = 509 nm, λ_{ex} = 350 nm)

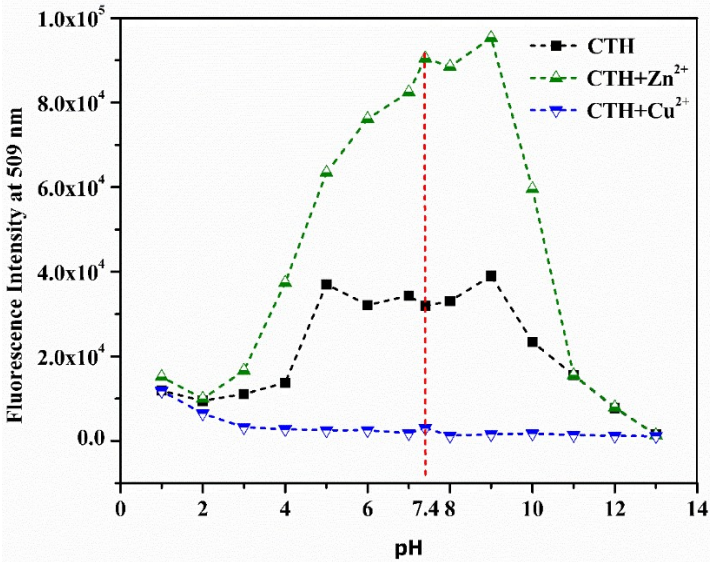

Fig. S20 Effect of pH variation on the fluorescence intensity of **CTH** (20 μM) in DMF:H_2O (3:7, v/v, pH 7.4) HEPES buffer solution, and after addition of Cu^{2+} and Zn^{2+} (20 μM), (λ_{em} = 509 nm, λ_{ex} = 350 nm).

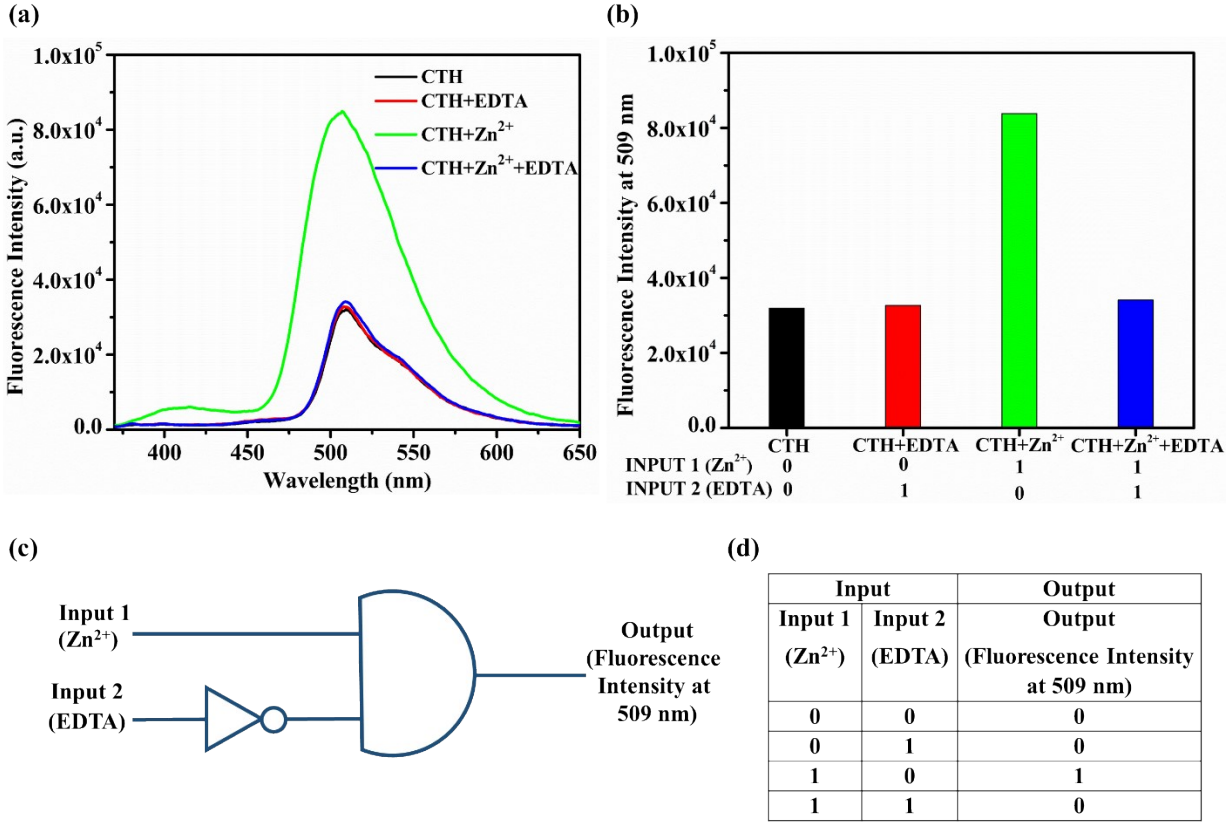

Input		Output
Input 1 (Zn^{2+})	Input 2 (EDTA)	Output (Fluorescence Intensity at 509 nm)
0	0	0
0	1	0
1	0	1
1	1	0

Fig. S21 (a) Fluorescence intensity variation of **CTH** in the absence and presence of Zn^{2+} and EDTA (λex = 350 nm); **(b)** histogram showing emission output at 509 nm; **(c)** schematic representation of INHIBIT logic gate; **(d)** truth table.

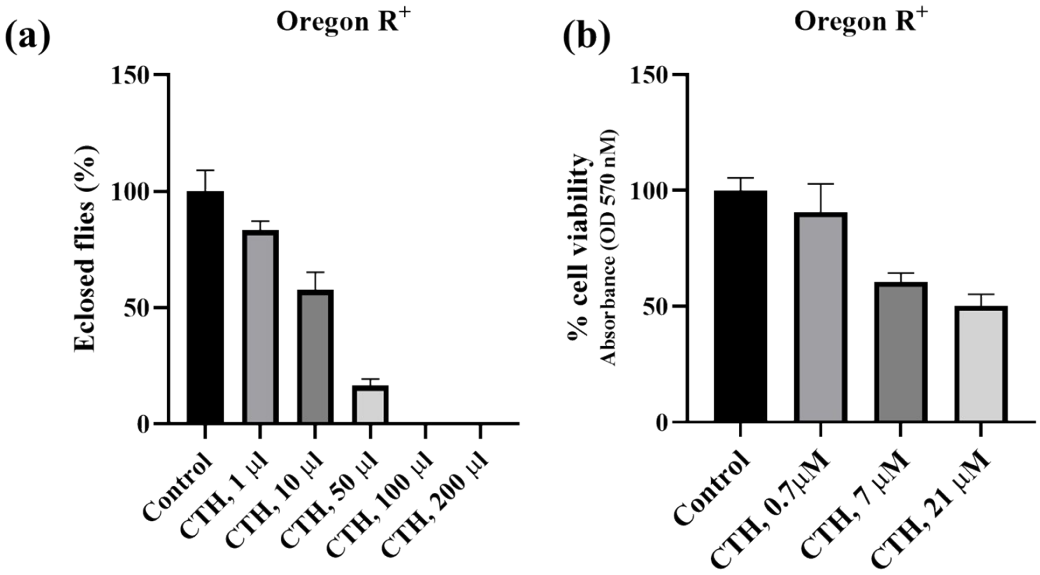

Fig. S22 (a) Histogram showing the percentage of wild-type flies that eclosed during the toxicity assay after **CTH** treatment. **(b)** Histogram illustrating the percentage of cell viability following the MTT assay of **CTH**-treated wild-type larval gut tissue.

Table S1 Fluorescence decay parameters and quantum yields of **CTH** in ethanol-water mixtures at different fraction of water

f_w	A	τ (ns)	<τ> (ns)	ϕ	K_r($^{-}$s)	K_{nr}($^{-}$s)
f_w=70%	0.802(A_1)	0.308(τ_1)	0.595	1.19 x 10^{-3}	2.01 x 10^6	16.79 x 10^8
	0.123(A_2)	2.472(τ_2)				
f_w=99%	0.474(A_1)	0.991(τ_1)	1.866	8.50 x 10^{-3}	4.55 x 10^6	5.31 x 10^8
	0.233(A_2)	3.645(τ_2)				

Table S2 Fluorescence decay parameters of **CTH** in ethanol-glycerol mixtures at different fraction of glycerol.

f_w	A	τ (ns)	<τ> (ns)
f_w=50%	0.471(A_1)	0.526(τ_1)	0.526
	0.471(A_2)	0.526(τ_2)	
f_w=90%	0.712(A_1)	0.608(τ_1)	0.703
	0.027(A_2)	3.215(τ_2)	

Table S3 Fluorescence decay parameters and quantum yields of **CTH** before and after treatment with Zn^{2+}/Cu^{2+} in DMF:H_2O (3:7, v/v, pH 7.4) HEPES buffer solution

Sample	A	τ (ns)	<τ> (ns)	ϕ	K_r($^-$s)	K_{nr}($^-$s)
CTH	0.408(A_1)	2.798(τ_1)	1.666	6.64 x 10^{-3}	3.99 x 10^6	5.96 x 10^8
	0.474(A_2)	0.691(τ_2)				
CTH-Zn^{2+}	0.475(A_1)	3.598(τ_1)	2.856	20.63 x 10^{-3}	7.22 x 10^6	3.43 x 10^8
	0.223(A_2)	1.273(τ_2)				
CTH-Cu^{2+}	0.202(A_1)	3.104(τ_1)	0.970	1.75 x 10^{-3}	1.81 x 10^6	10.29 x 10^8
	0.862(A_2)	0.471(τ_1)				

Table S4 Crystallographic data for **CTH**-Cu^{2+}

Empirical formula	$C_{20}H_{25}CuF_6N_2O_7PS_3$
Formula weight	710.11
Temperature (K)	293(2)
Wavelength (Å)	0.71073
Crystal system	triclinic
Space group	P-1
a (Å)	9.5284(3)
b (Å)	12.9129(12)
c (Å)	13.4689(5)
α (º)	114.553(3)
β (º)	99.864(3)
γ (º)	90.546(2)
Volume (Å^3)	1435.17(9)
Z	2
Density (g/cm^3)	1.643
μ (mm^{-1})	1.116
F(000)	722.0
Crystal size (mm)	0.25 × 0.15 × 0.1

θ range for data collection (º)	4.978 to 114.314
No. of reflections collected	29943
No. of independent reflections (R_{int})	9270 (0.0534)
Number of data/restraints/parameters	9270/318/368
Goodness-of-fit on F^2	1.073
R_1, wR_2 [a,b][(I>2σ(I))]	0.0779, 0.2268
R_1, wR_2[a,b] (all data)	0.1199, 0.2561
Largest difference in peak and hole (e.Å^{-3})	1.62 and -0.61

[a] $R_1 = \Sigma||F_o| - |Fc||\Sigma|F_o|$. [b] $R_2 = [\Sigma w(|F^2_o| - |F^2_c|)^2/\Sigma w|F^2_o|^2]^{1/2}$

Table S5 Bond Lengths for **CTH**-Cu^{2+}

Bonds	Length/Å	Bonds	Length/Å
Cu1- O**3**	1.936(3)	O3- C9	1.230(6)
Cu1- O4	1.908(4)	O4- C12	1.294(6)
Cu1- O6	1.957(3)	N1- N2	1.383(5)
Cu1- N1	1.940(4)	N1- C10	1.306(6)
Cu1- O5	2.281(4)	C10- C8	1.472(6)
S2- O6	1.528(4)	O2- C5	1.394(6)
N2- C12	1.321(6)	O2- C9	1.356(6)

Table S6 Bond Angles for **CTH**-Cu^{2+}

Bonds	Angle/°	Bonds	Angle/°
O3- Cu1- O6	89.66(14)	N2- N1- Cu1	112.7(3)
O3- Cu1- N1	92.07(15)	C10- N1- Cu1	130.7(3)
O3- Cu1- O5	89.45(18)	C10- N1- N2	116.7(4)
O4- Cu1- O3	171.49(16)	C12- C13- S1	122.2(4)
O4- Cu1- O6	94.24(14)	C12- C13- C14	123.8(4)
O4- Cu1- N1	82.49(15)	N1- C10- C8	119.8(4)
O4- Cu1- O5	97.87(18)	N1- C10- C11	122.2(5)
O6- Cu1- O5	92.97(17)	C8- C10- C11	117.9(4)
N2- C12- C13	116.6(4)	N1- Cu1- O6	167.42(17)
C13- S1- C16	92.1(3)	N1- Cu1- O5	99.50(17)

Table S7 Detection of Zn^{2+} and Cu^{2+} in real water samples

Sample	Added Zn^{2+} (μM)	Detected Zn^{2+} (μM)	Recovery (%)	Added Cu^{2+} (μM)	Detected Cu^{2+} (μM)	Recovery (%)
Ganga river	1	1.13	113.00	1	1.19	119.00
	5	7.03	140.60	5	6.01	120.20
Pond 1	1	0.98	98.00	1	1.23	123.33
	5	7.10	142.00	5	7.42	148.40
Pond 2	1	1.04	104.67	1	0.99	99.00
	5	6.33	126.60	5	6.5	130.00

Table S8 Comparison of **CTH** with past reported probe

Metal ions/ Solvent	Binding constant	Detection limit (LOD)	Ref.
Zn^{2+}, Cu^{2+} $CH_3OH:H_2O(2:3)$	Zn^{2+}: 4.2×10^4 M^{-1} Cu^{2+}: 2.6×10^4 M^{-1}	Zn^{2+}: 10^{-6} M Cu^{2+}: 10^{-5} M	11
Zn^{2+}, Cu^{2+} DMSO:water (1:1)	Zn^{2+}: 3.93×10^4 M^{-1} Cu^{2+}: 3.77×10^5 M^{-1}	Zn^{2+}: 3.5×10^{-8} M Cu^{2+}: 1.46×10^{-6} M	12
Zn^{2+}, Cu^{2+} $THF:H_2O$ (5:95)	Zn^{2+}: 8.70×10^4 M^{-1} Cu^{2+}: 3.13×10^5 M^{-1}	Zn^{2+}: 1.8×10^{-6} M Cu^{2+}: 2.3×10^{-7} M	13
Zn^{2+}, Cu^{2+} CH_3CN	Zn^{2+}: 1.31×10^4 M^{-1} Cu^{2+}: 2.45×10^2 M^{-1}	Zn^{2+}: 2.41×10^{-6} M Cu^{2+}: 4.23×10^{-6} M	14
Zn^{2+}, Cu^{2+} $CH_3OH:H_2O$ (4:1, pH 7.2) HEPES	Zn^{2+}: 1.05×10^6 M^{-1} Cu^{2+}: 1.16×10^8 M^{-1}	Zn^{2+}: 7.19×10^{-8} M Cu^{2+}: 5.53×10^{-7} M	15
Zn^{2+}, Cu^{2+} Methanol: H_2O (9:1, pH = 7.4)	Zn^{2+}: 4.35×10^6 M^{-1} Cu^{2+}: N/A	Zn^{2+}: 3.21×10^{-8} M Cu^{2+}: 2.13×10^{-8} M	16
Zn^{2+}, Cu^{2+} $DMF:H_2O$ (3:7, pH 7.4) HEPES	Zn^{2+}: 1.07×10^5 M^{-1} Cu^{2+}: 1.70×10^5 M^{-1}	Zn^{2+}: 2.97×10^{-9} M Cu^{2+}: 6.75×10^{-9} M	**This work**

References

1. R. H. Vekariya and H. D. Patel, Synth. Commun., 2014, **44**, 2756–2788.
2. J. Luo, Z. Xie, Z. Xie, J. W. Y. Lam, L. Cheng, H. Chen, C. Qiu, H. S. Kwok, X. Zhan, Y. Liu, D. Zhu and B. Z. Tang, *Chem. Commun.*, 2001, **18**, 1740–1741.
3. K. R. Barqawi, Z. Murtaza and T. J. Meyer, *J. Phys. Chem.*, 1991, **95**, 47–50.
4. G. L. Long and J. D. Winefordner, *Am. Chem. Soc.*, 1983, **55**, 712A–724A.
5. H. A. Benesi and J. H. Hildebrand, *J. Am. Chem. Soc.*, 1949, **71**, 2703–2707.
6. A. D. Becke, J. Chem. Phys, 1993, **98**, 5648–5652.
7. G. A. Petersson and A.-L. Mohammad A, *J. Chem. Phys.*, 1991, **9**, 6081–6090.
8. O. V. Dolomanov, L. J. Bourhis, R. J. Gildea, J. A. K. Howard and H. Puschmann, *J. Appl. Crystallogr.*, 2009, **42**, 339–341.
9. G. M. Sheldrick, *Acta Crystallogr. Sect. C Struct. Chem.*, 2015, **71**, 3–8.
10. L. J. Farrugia, *J. Appl. Crystallogr.*, 1997, **30**, 565.
11. 42 N. Roy, S. Nath, A. Dutta, P. Mondal, P. C. Paul and T. S. Singh, RSC Adv., 2016, **6**, 63837–63847.
12. J. S. Ganesan, S. Gandhi, K. Radhakrishnan, A. Balasubramaniem, M. Sepperumal and S. Ayyanar, Spectrochim. Acta A, 2019, **219**, 33–43.
13. B. Zha, S. Fang, H. Chen, H. Guo and F. Yang, Spectrochim. Acta A, 2022, **269**, 120765.
14. R. Arabahmadi, J. Photochem. Photobiol. A Chem., 2022, **426**, 113762.
15. M. Yang, Y. Zhang, W. Zhu, H. Wang, J. Huang, L. Cheng, H. Zhou, J. Wu and Y. Tian, J. Mater. Chem. C, 2015, **3**, 1994–2002.
16. P. Das, S. S. Rajput, M. Das, S. Laha, I. Choudhuri, N. Bhattacharyya, A. Das, B. C. Samanta, M. M. Alam and T. Maity, J. Photochem. Photobiol. A Chem., 2022, **427**, 113817.